ELSEVIER

Chemical Engineering Journal 72 (1999) 117–124

Chemical Engineering Journal

Drop breakage in stirred tanks with Newtonian and non-Newtonian fluid systems

K. Shimizu, K. Minekawa, T. Hirose, Y. Kawase*

Biochemical Engineering Research Center, Department of Applied Chemistry, Toyo University, Kawagoe, Saitama 350-8585, Japan

Received 15 June 1998; received in revised form 17 October 1998; accepted 30 October 1998

Abstract

Drop size distributions were measured in agitated non-Newtonian fluid systems using a 0.09 m diameter mechanically stirred tank. The dispersion process was carried out in the absence of coalescence by keeping the dispersed phase volume fraction at less than 0.005. Aqueous solutions of carboxymethyl cellulose and xanthan gum were used as the continuous phase with palm oil forming the dispersed phase. Additionally, agar solutions were used as the dispersed phase with salad oil as the continuous phase, which is weakly non-Newtonian. It was experimentally found that the non-Newtonian characteristics of the continuous phase caused an increase in the maximum drop size, particularly at low impeller speeds and wide drop size distributions. The Sauter drop diameter was proportional to the maximum drop diameter in non-Newtonian and Newtonian fluid systems. Models for drop breakage in a stirred tank have been developed to account for the effect of non-Newtonian flow behaviour. The boundary-layer shear force concept was applied to discuss the influence of non-Newtonian flow behaviour on the shear stress acting on the drop and drop break-up in a stirred tank. It was found that the experimental data correspond to the boundary-layer shear force models in non-coalescing systems.

Keywords: Drop breakage; Non-Newtonian fluid; Boundary-layer shear force concept; Stirred tank

1. Introduction

In the chemical, biochemical, food and pharmaceutical industries, two-liquid-phase dispersion is a process of considerable importance [1]. The dispersions are commonly formed by mechanical agitation of the liquid–liquid systems. The size of the drops and their dynamics play a very important role in the mass transfer and chemical reactions taking place in a stirred tank [1–3]. Therefore, the literature on the relationship between drop size, physical properties and operating conditions, including agitation speed, is very extensive. However, most of the information available relates only to Newtonian systems. Lagisetty et al. [4] and Koshy et al. [5] discussed the effect of non-Newtonian flow behaviour of the dispersed phase on drop breakage. The non-Newtonian behaviour of the continuous phase has not been studied, except for the work of Boye et al. [3], in which the increase in the apparent viscosity of the dispersion due to the increase in the dispersed phase concentration was investigated. Although non-Newtonian fluids are frequently encountered, information available on drop break-up in non-Newtonian liquid systems is limited. In particular, little published work is available on the aspect of the non-Newtonian flow behaviour of the continuous phase. The turbulent eddy drop break-up mechanism gives a good description of the maximum drop diameter provided that the flow in the stirred tank is fully turbulent [6–8]. However, there are many situations in which the flow is not fully turbulent. In particular, when the continuous phase is viscous, the intensity of turbulence is insufficient to justify the application of the Kolmogoroff theory of isotropic turbulence [3]. The boundary-layer shear force model is based on the mechanism in which drop break-up is considered to occur in the boundary layer on the impeller surface. This concept has been examined by several investigators [9–13]. Their work was limited to systems in which the continuous phase is Newtonian. No model has been proposed for drop break-up in stirred tanks with non-Newtonian continuous phases in the available literature. It is clear, therefore, that more experimental and theoretical studies for drop breakage in non-Newtonian fluid systems are desirable.

The present study focuses on the effect of continuous phase non-Newtonian flow behaviour on drop breakage. Drop sizes and drop size distributions are measured in non-Newtonian fluid systems. In general, the drop size

*Corresponding author. Tel.: +81-492-39-1377; fax: +81-492-31-1031; e-mail: bckawase@eng.toyo.ac.jp

1385-8947/99/$ – see front matter
PII: S1385-8947(98)00150-8

distribution obtained in a stirred tank is the result of drop breakage and coalescence occurring simultaneously. In the present study, however, the dispersed phase volume fraction is limited to less than 0.005; therefore, the dispersion process is assumed to be mainly controlled by the break-up of drops. Models are developed for drop breakage in non-Newtonian liquid systems on the basis of the boundary-layer shear force mechanism and their applicability is examined using the present experimental data and the available correlations for the maximum drop sizes.

2. Experimental details

Experiments were conducted in a 0.090 m internal diameter flat-bottomed polyvinyl chloride vessel under fully baffled conditions. A schematic diagram of the apparatus, including all dimensions, is given in Fig. 1. Agitation was provided by a six-flat-blade stainless steel Rushton turbine impeller of 0.049 m in diameter. It was positioned centrally in the stirred tank at a distance of $0.5D_T$ from the base of the tank. The impeller speed was varied from 3.75 to 11.7 s^{-1}. The liquid temperature in the tank was controlled at 323.15 ± 0.5 K.

Table 1 summarizes the physical properties of the liquids used in this work. Aqueous solutions of carboxymethyl cellulose (CMC) and xanthan gum (XG) were used to study the effect of non-Newtonian flow behaviour of the continuous phase. Rheological measurements were carried out using a coaxial cylinder viscometer (Fann Instrument, Model 35) at shear rates of 1.5–3254 s^{-1}. The rheological properties were assumed to be represented by a power-law model

$$\tau = K\dot{\gamma}^n \quad (1)$$

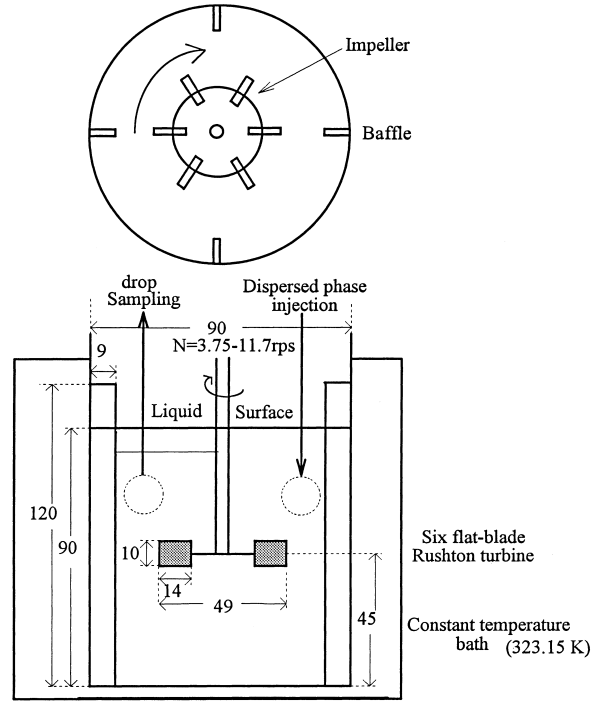

Fig. 1. Schematic diagram of the stirred tank. Dimensions in millimeters.

This flow model has been widely used for shear dependent viscosity, i.e. shear thinning ($n < 1$) and shear thickening ($n > 1$). When $n = 1$, Eq. (1) represents Newtonian viscosity and K is equivalent to μ. The agar solutions, which were used to examine the influence of dispersed-phase viscous forces on the mean drop size and drop size distribution, also represented weakly non-Newtonian flow behaviour. Interfacial tension was measured by the falling drop method [11]. In order to achieve the equilibrium drop size, the mixing was

Table 1
Properties of continuous and dispersed phases at 323.15 ± 0.5 K

	Continuous phase					Dispersed phase			
	ρ_c (kg m−3)	n_c	K_c (Pa s^n)	σ (N m^{-1})	μ_c (Pa s)	ρ_d (kg $^{-3}$)	μ_d (Pa s)	n_d	K_d (Pa s^n)
System I									
Palm oil						891	0.0222		
Water	988	1	0.0005	0.0201					
Glycerol	1245	1	0.145	0.0135					
0.01%CMC	988	0.913	0.0036	0.0200					
0.05%CMC	988	0.650	0.0483	0.0199					
0.10%CMC	988	0.635	0.0835	0.0196					
0.15%CMC	989	0.614	0.131	0.0195					
0.20%CMC	989	0.604	0.173	0.0194					
0.50%CMC	991	0.544	0.655	0.0189					
0.01%XG	988	0.757	0.0069	0.0200					
0.25%XG	989	0.436	0.374	0.0192					
0.50%XG	991	0.265	2.10	0.0189					
System II									
2% Agar solution						999		0.840	0.039
Salad oil	901			0.0126	0.0205				

run for at least 1 h before sampling the suspension [8,11,14]. In order to confirm that a steady state was attained, samples were drawn from the vessel at every 30 min for 3 h. It was found that, in this experiment, the time required to achieve a steady state was about 1 h as in previous investigations [8,11,14]. The siphoned sample was poured into iced water or cold salad oil to freeze the drops rapidly [7,15]. The photographic system consisted of a CCD camera, and a microscope was used to measure the drop sizes. A minimum of 200 drops were examined to establish the values of the maximum drop diameter D_{max} and the Sauter mean drop diameter D_{32} and the drop size distributions [4,14,16,17]. The dispersed phase volume fraction was limited to $\phi < 0.005$ to ensure that a dilute non-coalescing suspension resulted [8].

3. The boundary-layer shear force model

Hinze [6] established a basis for drop break-up in which surface and dispersed phase viscous forces contribute to drop stability

$$\tau \geq \frac{\left(\sigma + \mu_d \sqrt{\tau/\rho_d}\right)}{D} \tag{2}$$

This relationship indicates that the shear stress imposed by the continuous phase acts to deform a drop and to break it when the counter-balancing surface tension forces and viscous stresses inside the drop are overcome. Eq. (2) has been widely used to develop correlations for an estimation of the maximum drop diameter. Many expressions have been proposed for the shear stress depending on whether the continuous phase is laminar or turbulent. For fully turbulent flow conditions, the turbulent eddy drop break-up mechanism is very useful for predicting the drop size. There are many situations in which the flow field is not fully turbulent. In general, drop breakage mainly occurs in a small zone outside the edge of the impeller in a stirred tank [11]. The impeller would be expected to have the highest shear rate. We have assumed that the boundary layer around the blades of a rotating Rushton turbine controls the drop break-up and have developed a model based on this mechanism. Since the minimization of coalescence events is accomplished by maintaining low dispersed phase fractions, coalescence occurring in the region away from the impeller is not considered. Strong shearing in a boundary layer on the blade leads to drop break-up (Fig. 2). This mechanism has been examined by Boye et al. [3], Leng and Quarderer [9], Cherry and Papoutsakis [10] and Kumar et al. [11]. However, their examinations were not completed and, furthermore, were limited only to Newtonian continuous phase systems. We have developed a new model for drop breakage in non-Newtonian liquid continuous phase systems. It should be noted that a number of simplifying assumptions are made because of the complex flow field in the vicinity of the impellers.

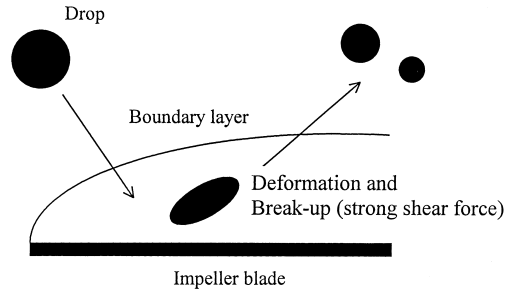

Fig. 2. Drop break-up in the boundary layer (boundary-layer shear force model).

It has been pointed out [18–20] that the dispersed phase viscosity has a significant influence on the maximum drop size. Therefore, we consider the following relationship instead of Eq. (2)

$$\tau \geq \frac{\left[\sigma + f(\mu_d/\mu_c)\mu_d \sqrt{\tau/\rho_d}\right]}{D} \tag{3}$$

The viscosity ratio function $f(\mu_d/\mu_c)$ is additionally introduced to the viscous stress term [14]. By considering the deformation of the drops in shear flow [21] and the motion of the drops [22], the function of the ratio of viscosity is assumed to be

$$f\left(\frac{\mu_d}{\mu_c}\right) = \frac{1 + 1.5(\mu_d/\mu_c)}{1 + (\mu_d/\mu_c)} \tag{4}$$

This relationship suggests that the maximum drop size increases with increasing μ_d/μ_c or μ_d. This trend coincides with the experimental results obtained by Nishikawa et al. [23] and the model proposed by Lagisetty et al. [4]. The dispersed phase viscosity has a stabilizing effect on the deformation and break-up of drops. In the limit $\mu_d \to 0$, we have $f(\mu_d/\mu_c) = 1$ and Eq. (3) yields Eq. (2). For $\mu_d \to \infty$, we obtain $f(\mu_d/\mu_c) = 1.5$. The range of the viscosity ratio correction factor reported by Davies [19] is from 0.7 to 1.4. In order to take into account non-Newtonian flow behaviour in Eqs. (2)–(4), μ is replaced by μ_{app} based on Metzner and Otto's [24] concept of an average shear rate

$$\mu_{app} = K(k_s N)^{n-1} \tag{5}$$

The proportionality constant k_s is generally dependent on the impeller geometry and is given by Skelland [25].

The maximum shear stress on the drop surface for Newtonian liquid systems has been evaluated to be three times the average shear stress [10]

$$\tau_{laminar} = 3\mu_c \dot{\gamma} \tag{6}$$

On the basis of the above relationship, we assume that the shear stress responsible for drop break-up in non-Newtonian liquid systems may be written as

$$\bar{\tau}_{laminar} = 3\tau_{laminar} = 3K_c \dot{\gamma}^{n_c} = 3K_c \left(\frac{U}{\delta_{laminar}}\right)^{n_c} = 3K_c \left(\frac{\pi N D_I}{\delta_{laminar}}\right)^{n_c} \tag{7}$$

where the laminar boundary layer thickness δ is given as [25]

$$\delta_{\text{laminar}} = \left\{\frac{280}{39}(n_c+1)\left(\frac{3}{2}\right)^{n_c}\right\}^{1/(n_c+1)} \times \left\{\frac{x^{n_c}(\pi N D_I)^{2-n_c}\rho_c}{K_c}\right\}^{-1/(n_c+1)} x \quad (8)$$

The characteristic liquid velocity U and length x are assumed to be the liquid velocity at the tip of the disk $\pi N D_I$ and the impeller blade width, respectively. Using Eqs. (3), (7) and (8), we can estimate the maximum drop size D_{max} in non-Newtonian laminar liquid systems. In the boundary layer on the blade, a drop experiences strong shearing action, leading to its breakage provided that the drop diameter is smaller than the boundary layer thickness.

The drop passing through the turbulent boundary layer may experience a different shear stress compared with the laminar boundary layer. The shear stress in the non-Newtonian turbulent boundary layer may be written as [25]

$$\tau_{\text{turbulent}} = \Omega\rho_c^{1-\beta}\left\{8^{n_c-1}K_C\left(\frac{3n_c+1}{4n_c}\right)^{n_c}\right\}^{\beta} \times \delta_{\text{turbulent}}^{-\beta n_c}(\pi N D_I)^{2-\beta(2-n_c)} \quad (9)$$

The boundary layer thickness is written as

$$\delta_{\text{turbulent}} = \left[\frac{(\beta n_c+1)\Omega}{\Psi}\left\{8^{n_c-1}\left(\frac{3n_c+1}{4n_c}\right)^{n_c}\right\}^{\beta} \times \left\{\frac{x^{n_c}(\pi N D_I)^{2-n_c}\rho_c}{K_c}\right\}^{-\beta}\right]^{1/\beta n_c+1} x \quad (10)$$

where

$$\Psi = \frac{2-\beta(2-n_c)}{2(1-\beta+\beta n_c)} - \frac{2-\beta(2-n_c)}{2-2\beta+3\beta n_c}$$

and

$$\Omega = \frac{\alpha(0.817)^{2-\beta(2-n_c)}}{2^{\beta n_c+1}}$$

The values of α and β in the above equations, which are functions of the flow index n, and are given in the figures presented by Dodge and Metzner [26], are approximately represented by the following equations

$$\alpha = \left(\frac{n_c}{10^{10.278}}\right)^{1/9.2767} \quad (11)$$

and

$$\beta = 0.25058 n_c^{-0.21981} \quad (12)$$

The shear stress responsible for drop break-up in the turbulent boundary layer on the blade may be written as

$$\bar{\tau}_{\text{turbulent}} = C\tau_{\text{turbulent}} \quad (13)$$

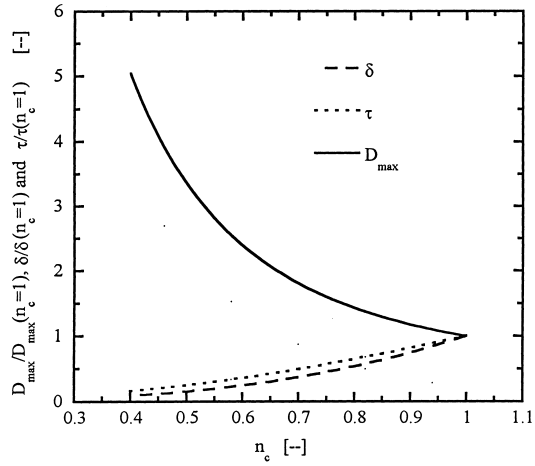

Fig. 3. Effects of non-Newtonian flow behaviour on D_{max}, τ and δ in the low Reynolds number region ($x = 0.014$ (m), $D_I = 0.049$ (m), $N = 10$ (s^{-1}), $K_c = 1.0$ (Pa s^n), $\rho_c = 988$ (kg m^{-3}), $\mu_d = 0.0005$ (Pa s), $\rho_d = 0.0222$ (kg m^{-3}), $\sigma = 0.0200$ (N m^{-1})).

The turbulent boundary layer on the blade may be very complicated in a highly chaotic fashion [11]. At any location along the blade, the shear rates in a direction perpendicular to the blade, as well as in the direction along the blade, are disturbed in a highly non-linear fashion. In the literature, moreover, the turbulent intensity factor near the impeller tip where the break-up process occurs is between 8 and 70 [17]. Therefore, the proportionality coefficient C in the above equation was tentatively assumed to be

$$C = 50\left[7\times10^{-4}n_c\left\{\frac{x^{n_c}(\pi N D_I)^{2-n_c}\rho_c}{K_c}\right\}\right]^{\{9n_c^3(n_c-1)\}} \quad (14)$$

For $n_c = 1$ (Newtonian fluids), $C = 50$. It is difficult to determine the value of C through a simple analysis because of the complicated liquid flow field in a stirred tank, especially around the blades of the impeller at high Reynolds numbers. Consequently, the resulting adjustable parameter C for turbulent flows was rather complicated.

Fig. 3 shows the variation of D_{max} with the flow index n for the laminar flow region. For reference, the effects of the flow index on the boundary layer thickness δ and shear stress τ are also presented in Fig. 3. The model predicts that the maximum drop diameter will increase with increasing shear thinning or decreasing flow index in the laminar flow region. With increasing shear thinning, the shear stress tending to deform the drop decreases and, as a result, the maximum drop diameter increases, as well as the predictions for the high Reynolds number region.

4. Results and discussion

Figs. 4 and 5 show the maximum drop diameter for low Reynolds numbers plotted against the impeller speed. As the impeller speed increases, the maximum drop size decreases. Fig. 4 shows a comparison between the experimental results

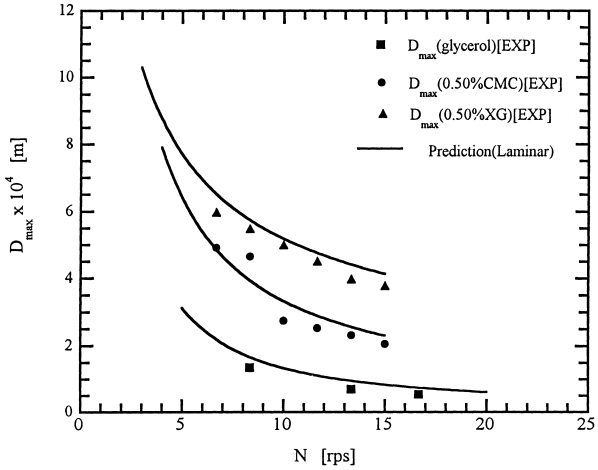

Fig. 4. Maximum drop diameter as a function of the impeller speed for the palm oil (dispersed)–glycerol (continuous), –0.5%CMC and –0.50%XG system.

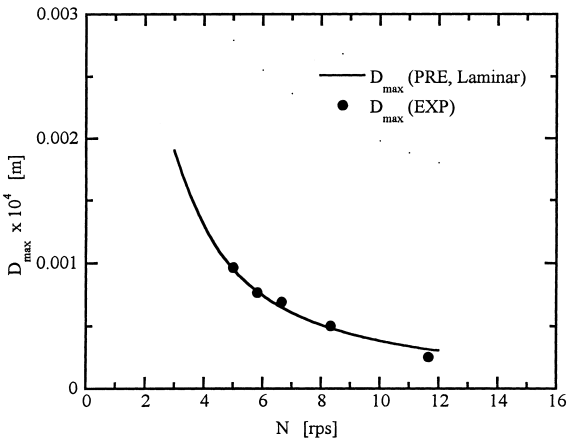

Fig. 5. Maximum drop diameter as a function of the impeller speed for the agar solution (dispersed)–salad oil (continuous) system.

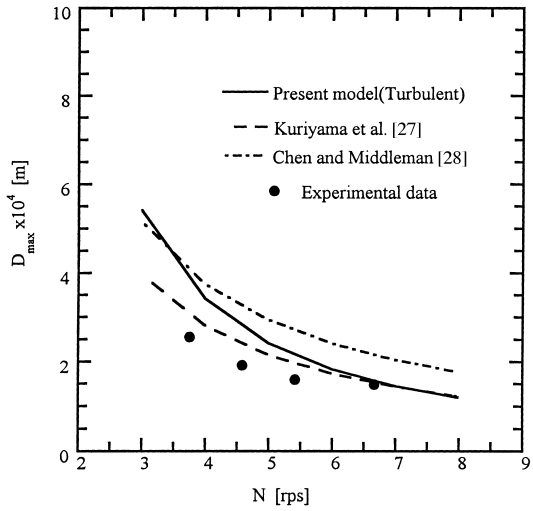

Fig. 6. Maximum drop diameter as a function of the impeller speed for the palm oil (dispersed)–water (continuous) system.

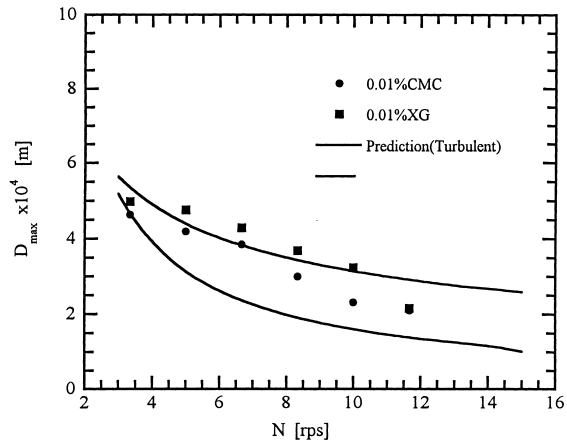

Fig. 7. Maximum drop diameter as a function of the impeller speed for the palm oil (dispersed)–0.01%CMC (continuous) and –0.01%XG system.

for $D_{\max}$ in the low Reynolds number region and the theoretical predictions. The results predicted by the proposed model, Eqs. (3), (7) and (8), are given by the full line. The agreement between the experimental results for glycerol, 0.50%CMC and 0.50%XG and the predictions of the model developed in this work is good. The range of the Reynolds number based on the blade width ($\mathrm{Re}_x = x^{n_c}(\pi N D_I)^{2-n_c}\rho_c/K_c$) for these systems is from 132 to 649. As shown in Fig. 5, the data for System II (2.0% agar solution (dispersed)–salad oil (continuous) system) also agree well with the predictions of the proposed model. For this system, the range of the Reynolds number ($\mathrm{Re}_x = x(\pi N D_I)\rho_d/\mu_{app\,d}$) is from 473 to 1040.

The comparisons of the experimental data at high Reynolds numbers for water, 0.01%CMC and 0.01%XG with the theoretical predictions obtained by Eqs. (3), (4), (9) and (10) are illustrated in Figs. 6 and 7. The full lines represent the results calculated from the proposed model. For water, the predictions of the turbulent boundary-layer stress model agree reasonably well.

In Fig. 6, for reference, the correlations for Newtonian fluids in the literature are also plotted. Chen and Middleman [27] obtained an empirical correlation for D_{32} as

$$\frac{D_{32}}{D_I} = 0.53\left(D_I^3 N^2 \frac{\rho_c}{\sigma}\right)^{-0.6} \tag{15}$$

Considering the values of $D_{\max}/D_{32}$ examined by Calabrese et al. [18], which are based on their data and the results of Chen and Middleman [27] and are given in Table 3 of their paper, we assumed that $D_{\max} = 1.67D_{32}$ and calculated $D_{\max}$ using the above equation.

Recently, Kuriyama et al. [28] proposed the following equation

$$8.7\times10^{-3}\mathrm{We}^{-1}\left(\frac{D_{32}}{D_I}\right)^{-5/3} + 1.1\times10^{-2}\mathrm{Re}^{-1}\mathrm{We}^{-1/2}\left(\frac{\mu_d}{\mu_c}\right) \times \left(\frac{\rho_c}{\rho_d}\right)^{1/2}\left(\frac{D_{32}}{D_I}\right)^{-13/6} = 1 \tag{16}$$

They also proposed

$$D_{max} = 1.6D_{32} \quad (17)$$

It is seen from Fig. 6 that the proposed model lies between the correlations of Chen and Middleman [27] (Eq. (15)) and Kuriyama et al. [28] (Eqs. (16) and (17)). The predictions obtained by the proposed model and the correlations of Chen and Middleman [27] and Kuriyama et al. [28] are in close agreement.

From Fig. 7, it can be seen that the experimental results for low viscosity solutions, 0.01%CMC and 0.01%XG, are in reasonable agreement with the theoretical predictions. The Reynolds number range for water is from 14 200 to 33 200, whereas that for dilute aqueous solutions of CMC and XG is from 2550 to 11 600. As described above, we assumed that the proportionality coefficient C in Eq. (13) was tentatively given by Eq. (14). In order to examine the generality of Eq. (14), more systematic studies may be required.

By assuming a linear relationship between D_{max} and D_{32} in the literature and fitting the present data, we obtain the following relationship (Fig. 8)

$$D_{max} = 1.67D_{32} \quad (18)$$

Fig. 8 shows that the linear relation is verified for Newtonian and non-Newtonian fluid systems in the whole Reynolds number region. The proportionality constant in the above correlation has been found to vary from 1.43 to 2.63 in the literature [14]. For Newtonian and non-Newtonian systems, experimental results confirm the assumption that the Sauter mean drop diameter is proportional to the maximum drop diameter. Furthermore, the proportionality constant seems to be independent of non-Newtonian flow behaviour.

Typical cumulative volume fractions for System I are given in Fig. 9(a)–(c). The figures indicate that the cumulative volume fraction curves move consistently to the left with impeller speed. This suggests that the drop breakage rate increases with impeller speed. By increasing the impeller speed or the shear stress, the cumulative volume fraction becomes narrow. Results for the drop size distribution are compared with the correlation obtained by Calabrese et al. [29]. They proposed the following correlation for the drop size distribution in Newtonian fluid systems

$$F_v\left(\frac{D}{D_{32}}\right) = 0.5\left\{1 + \mathrm{erf}\left(\frac{D/D_{32} - 1.07}{0.23\sqrt{2}}\right)\right\} \quad (19)$$

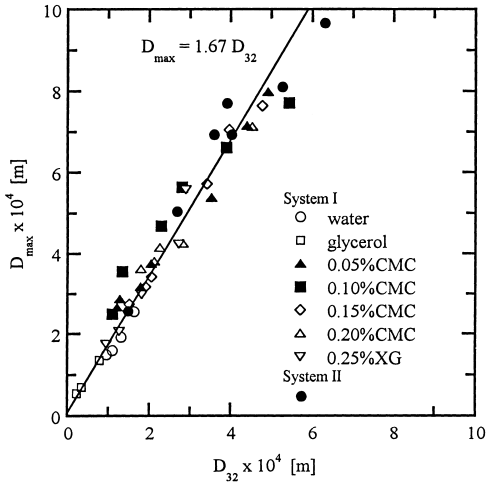

Fig. 8. D_{max} vs. D_{32}.

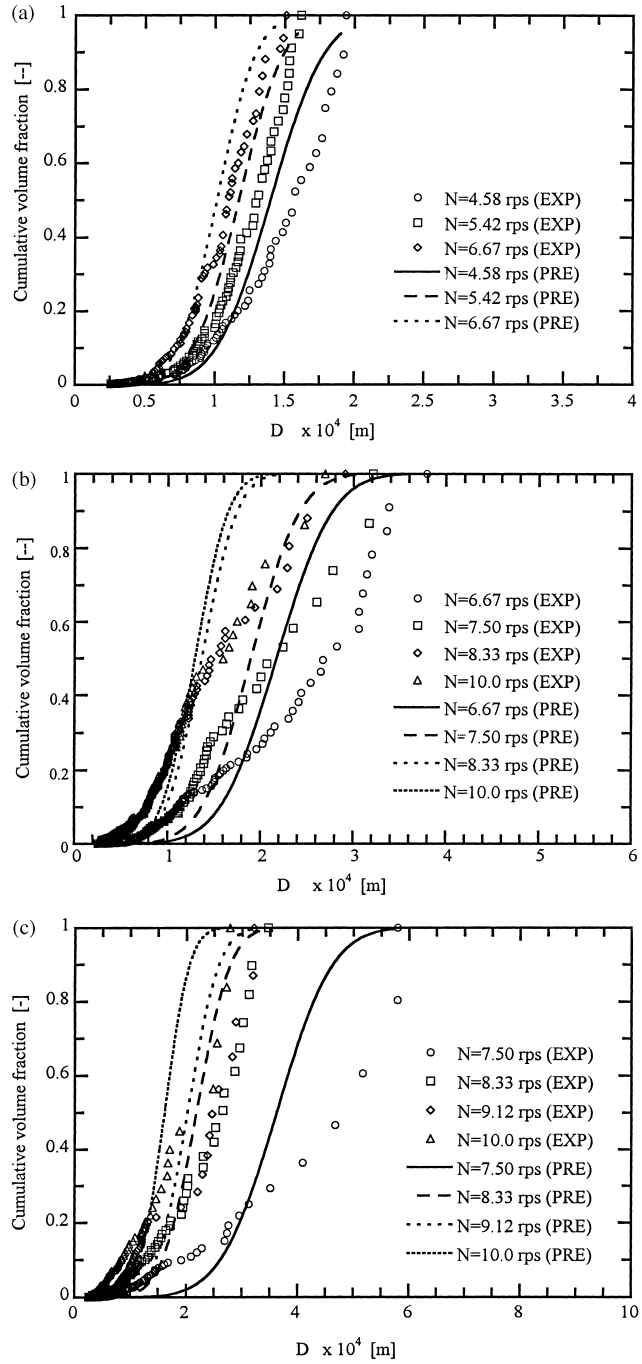

Fig. 9. (a) Drop size distribution for the palm oil (dispersed)–water (continuous) system. (b) Drop size distribution for the palm oil (dispersed)–0.05%CMC (continuous) system. (c) Drop size distribution for the palm oil (dispersed)–0.15%CMC (continuous) system.

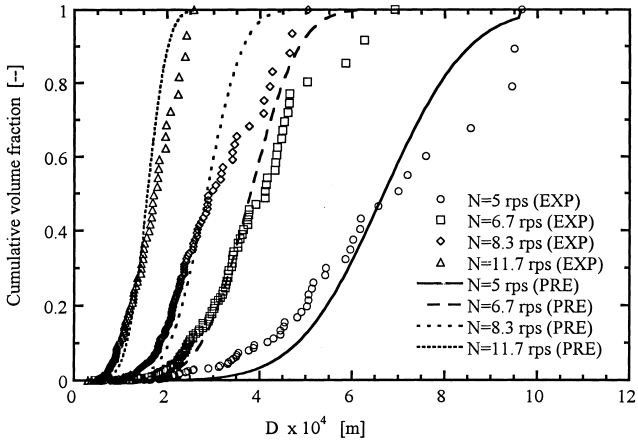

Fig. 10. Drop size distribution for the agar solution (dispersed)–salad oil (continuous) system.

It is seen from Fig. 9(a) that the drop size distributions for water are reasonably correlated by Eq. (19). For highly viscous non-Newtonian liquid systems, however, the drop size distributions considerably deviate from the predictions of Eq. (19) at lower impeller speeds, as shown in Fig. 9(b) and (c). This result suggests that non-Newtonian flow behaviour broadens the drop size distributions. The size of the smallest drops decreases, while their number increases. In non-Newtonian continuous phases, a drop usually breaks into rather large drops and very small drops, rather than equal-sized daughter drops, and long filaments or tails formed behind drops may also result in the formation of very small drops [30,31]. The size of the largest drops increases, while their number decreases. By maintaining low dispersed phase fractions, the minimization of coalescence events was assumed. However, some coalescence is expected to occur in the viscous non-Newtonian liquids. Additional experiments are in progress to examine stochastic drop break-up and coalescence in more detail and to develop a correlation for the drop size distributions for non-Newtonian systems. As shown in Fig. 10, the experimental data for D in System II agree well with the correlation of Calabrese et al. [29]. The non-Newtonian flow behaviour of the dispersed phase has an insignificant effect on the drop break-up for the systems used in this study.

5. Conclusions

Measurement of the drop sizes and drop size distributions in a stirred tank with non-Newtonian fluid systems was performed. By maintaining a low volume fraction of the dispersed phase, the drop sizes were assumed to depend on breakage and to be independent of coalescence. The maximum drop size increased with increasing non-Newtonian behaviour of the continuous phase. New models based on the boundary-layer shear stress mechanism have been developed for non-Newtonian laminar and turbulent flow fields. The proposed models for the laminar and turbulent flow regions were in reasonable agreement with the present experimental data for drop break-up in non-Newtonian systems. It may be concluded, therefore, that the proposed models suggested here will be useful for estimating shear stress and drop size in liquid–liquid dispersions under non-coalescing conditions for Newtonian and non-Newtonian fluid systems. It should be emphasized that idealizations have been made in the development of the models, because the actual flow is highly complicated. Experimental measurements confirm that the relationship between the Sauter mean drop diameter and the maximum drop diameter is linear and almost independent of the non-Newtonian flow behaviour. The proportionality coefficient found in this work is within the range of values reported in the available literature. The non-Newtonian flow behaviour of the continuous phase led to a widening of the drop size distribution. In order to define the region in which the proposed model for drop break-up is applicable, additional work is required. Discussion in this study is limited to dilute suspensions for which coalescence is negligible. For concentrated dispersions, however, break-up and coalescence of drops occur simultaneously. This problem will be studied in the future. Furthermore, experiments with alternative geometries are desirable. This study should be regarded as the first attempt to understand drop breakage in non-Newtonian fluid systems.

6. Nomenclature

C	proportionality coefficient in Eq. (13)
D	drop diameter (m)
D_I	impeller diameter (m)
D_{max}	maximum stable drop diameter (m)
D_T	tank diameter (m)
D_{32}	Sauter mean drop diameter (m)
F_v	cumulative volume frequency
$f(\mu_d/\mu_c)$	viscosity ratio correction factor
K	consistency index in a power-law model (Pa s^n)
k_s	proportionality constant in (5)
N	impeller speed (s^{-1})
n	flow index in a power-law model
U	velocity (m s^{-1})
x	impeller blade width (m)

Greek letters

α	function defined by Eq. (11)
β	function defined by Eq. (12)
δ	boundary layer thickness (m)
ϕ	volume fraction of dispersed phase
$\dot{\gamma}$	shear rate (s^{-1})
μ	viscosity (Pa s)
ρ	density (kg m^{-3})
σ	interfacial tension (N m^{-1})

τ	shear stress (Pa)
Ω	function used in Eq. (10)
Ψ	function used in Eq. (10)

Superscript

–	responsible for drop break-up

Subscripts

app	apparent
c	continuous phase
d	dispersed phase
EXP	experimental
laminar	laminar flow field
PRE	predicted
turbulent	turbulent flow field

References

[1] J.C. Godfrey, M.J. Slater, Liquid-Liquid Extraction Equipment, Wiley, Chichester, 1994.
[2] G.S. Laddha, T.E. Degaleesan, Transport Phenomena in Liquid Extraction, Tata McGraw-Hill, New Delhi, 1976.
[3] A.M. Boye, M.Y.A. Lo, P. Ayazi Shamlou, Chem. Eng. Commun. 143 (1996) 149–167.
[4] J.S. Lagisetty, P.K. Das, R. Kumar, K.S. Gandhi, Chem. Eng. Sci. 41 (1986) 65–72.
[5] A. Koshy, T.R. Das, R. Kumar, K.S. Gandhi, Chem. Eng. Sci. 43 (1988) 2625–2631.
[6] J.O. Hinze, AIChE J. 3 (1955) 289–295.
[7] R. Shinnar, J. Fluid Mech. 10 (1961) 259–275.
[8] F.B. Sprow, Chem. Eng. Sci. 22 (1967) 435–442.
[9] D.E. Leng, G.J. Quarderer, Chem. Eng. Commun. 14 (1982) 177–201.
[10] R.S. Cherry, E.T. Papoutsakis, Bioprocess Eng. 1 (1986) 29–41.
[11] S. Kumar, R. Kumar, K.S. Gandhi, Chem. Eng. Sci. 46 (1991) 2483–2489.
[12] A.M. Boye, P. Ayazi Shamlou, Annual ChemE Research Event 1 (1994) 495–497.
[13] K. Wichterle, Chem. Eng. Sci. 22 (1995) 3581–3586.
[14] M. Zerfa, B.W. Brooks, Chem. Eng. Sci. 51 (1996) 3223–3233.
[15] M. Nishikawa, F. Mori, S. Fujieda, J. Chem. Eng. Jpn 20 (1987) 82–88.
[16] A. Koshy, R. Kumar, K.S. Gandhi, Chem. Eng. Sci. 44 (1989) 2113–2120.
[17] D.I. Collias, R.K. Prud'homme, Chem. Eng. Sci. 47 (1992) 1401–1410.
[18] R.V. Calabrese, T.P.K. Chang, P.T. Dang, AIChE J. 32 (1986) 657–666.
[19] J.T. Davies, Chem. Eng. Sci. 42 (1987) 1671–1676.
[20] P.K. Das, Chem. Eng. Technol. 19 (1996) 39–42.
[21] G.I. Taylor, Proc. Roy. Soc. (London) 138A (1932) 41–48.
[22] R. Clift, J.R. Grace, M.E. Weber, Bubbles, Drops and Particles, Academic Press, New York, 1978.
[23] M. Nishikawa, T. Kayama, S. Nishioka, S. Nishikawa, Chem. Eng. Sci. 49 (1994) 2379–2384.
[24] A.B. Metzner, R.E. Otto, AIChE J. 3 (1957) 3–10.
[25] A.H.P. Skelland, Non-Newtonian Flow and Heat Transfer, Wiley, New York, 1967.
[26] D.W. Dodge, A.B. Metzner, AIChE J. 5 (1959) 189–203.
[27] H.T. Chen, S. Middleman, AIChE J. 13 (1967) 989–995.
[28] M. Kuriyama, M. Ono, H. Tokanai, H. Konno, Trans IChemE, 74 Part A (1996) 431-437.
[29] R.V. Calabrese, C.Y. Wang, N.P. Bryner, AIChE J. 32 (1986) 677–681.
[30] A. Fararoui, R.C. Kintner, Trans. Soc. Rheol. 5 (1961) 369–380.
[31] R.P. Chhabra, Bubbles, Drops, and Particles in Non-Newtonian Fluids, CRC Press, Florida, 1993.